LASER INTERFEROMETER GRAVITATIONAL WAVE OBSERVATORY

LIGO Laboratory / LIGO Scientific Collaboration

LIGO-T070251-00-D *LIGO* Date

In vacuum scatterometer for LIGO

Andrea Conte, Riccardo DeSalvo

Distribution of this document:
LIGO Science Collaboration

This is an internal working note
of the LIGO Project.

California Institute of Technology
LIGO Project – MS 18-34
1200 E. California Blvd.
Pasadena, CA 91125
Phone (626) 395-2129
Fax (626) 304-9834
E-mail: info@ligo.caltech.edu

Massachusetts Institute of Technology
LIGO Project – NW17-161
175 Albany St
Cambridge, MA 02139
Phone (617) 253-4824
Fax (617) 253-7014
E-mail: info@ligo.mit.edu

LIGO Hanford Observatory
P.O. Box 1970
Mail Stop S9-02
Richland WA 99352
Phone 509-372-8106
Fax 509-372-8137

LIGO Livingston Observatory
P.O. Box 940
Livingston, LA 70754
Phone 225-686-3100
Fax 225-686-7189

http://www.ligo.caltech.edu/

I studied is the feasibility of an in-vacuum scatterometer for the LIGO interferometer to track the changes, and possibly help to identify the sources of time varying losses of power in the interferometer arm cavities.

Background

The Laser Interferometer Gravitational waves Observer (LIGO) will detect the ripples in space-time by using a laser interferometer, in which the time that light takes to travel between suspended mirrors is measured with high precision.

GW detection requires at least two widely separated detectors, working simultaneously, to rule out false signals and to confirm that a gravitational wave has passed through the Earth. The LIGO Livingston Observatory in Livingston, Louisiana(30°29′55″N, 90°44′54″W) and the LIGO Hanford Observatory, on the Hanford Nuclear Reservation (46°27′28″N, 119°24′35″W) , located near Richland, Washington, are separated by 3,002 km (1,876 miles). VIRGO (43°37′53″N, 10°30′18″E) is the third km class observatory of the network.

Since gravitational waves are expected to travel at the speed of light, these separations correspond to a difference in gravitational wave arrival times of up to ten milliseconds (twenty milliseconds for VIRGO). Through the use of triangulation, the difference in arrival times can determine the source of the wave in the sky.

Each observatory supports an L-shaped ultra high vacuum system, measuring 4 kilometres (3 km for VIRGO) on each side.

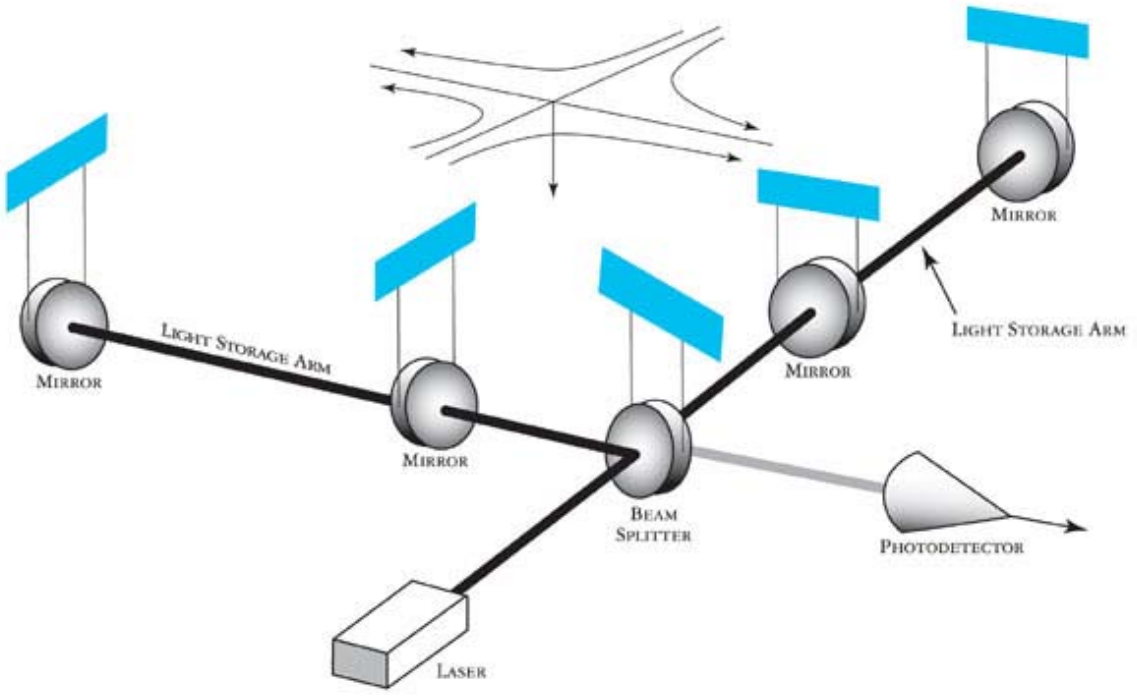

Figure 1: Schematic of the LIGO optical configuration.

Each interferometer consists of mirrors suspended at each of the corners of the L; it is known as a power-recycled Michelson interferometer with Fabry-Perot arms (Fig. 1).

When a gravitational wave passes through the interferometer, the space-time in the local area is altered. Depending on the source of the wave and its polarization, this results in an effective change in the length of one or both of the cavities. After an equivalent of approximately 75 trips down the 4 km length to the far mirrors and back again, the two separate beams leave the arms and recombine at the beam splitter. The beams returning from two arms are kept out of phase so that when the arms are both in resonance, their light waves subtract, and no light should arrive at the photodiode. When a gravitational wave passes through the interferometer, the distances along the arms of the interferometer are shortened and lengthened, causing the beams to become slightly less

out of phase, so some light arrives at the photodiode synchronously with the wave, indicating a signal.

In actual operation, noise sources can cause movement in the optics which produces similar effects to real gravitational wave signals; a great deal of the art and complexity in the instrument is in finding ways to reduce these spurious motions of the mirrors.

Losses problem

The study is focussed on LIGO, but it is equally relevant for VIRGO.

Since the most important element of the interferometer is the main beam of the laser, it is of fundamental interest to make sure that the total power stored in the interferometer cavities isn't lost.

Various measurements with the aid of simulations [1] indicate that the total loss in the initial LIGO (I-LIGO) arm is around 150 ppm of the total power per arm or 75 ppm per mirror with the uncertainty of about 15 ppm. It is possible to account for these losses in different components: 20 – 30 ppm can be explained by the scattering loss due to mirror surface errors with spatial wavelength greater than a few millimetres, 3.5 ppm is the estimated transmission loss of ETM, 4 ppm the absorption loss, 1 – 2 ppm the diffractive loss and 4.6 ppm is due to microroughness contribution. The residual amount of losses (30 – 40 ppm) is still unknown; unaccounted scattering is the main suspect.

The same considerations can be made for Advanced LIGO (Ad-LIGO), which has been proposed to improve the sensitivity of the interferometer by a factor of 10 compared to I-LIGO.

Ad-LIGO needs to reduce the arm losses by a factor of 2. Considering that the unreduceable estimated losses amount to 35 ppm per arm mirror, there are only 7 ppm residual from both microroughness contributions and other unknown losses. Thus, it can be realized that the unknown losses present in I-LIGO are mysteriously disappeared in Ad-LIGO.

Various efforts are going on in order to uncover the source of the unknown losses of the I-LIGO mirror, and most of them are focusing on a better evaluation of the microroughness contribution.

Part of those losses may be due to scatterers or films that deposit on the mirror after production and even after the mirror is installed in the vacuum system. We propose a monitoring system sensitive to such events, and to the size of the loss-inducing agent, that could help distinguish between films and particles and give a rough idea of the average particulate size.

Mathematical approach

To understand how to face the problem of light scattering from a surface we should find some relations which are able to mathematically connect the back scattered light to the surface imperfections of the mirror.

For this purpose, suppose to have a mirror whose surface is characterized by a roughness, which can be described by the following function,

$$S = a \sin(k_x x)$$

where a is the amplitude of the deformation and $k_x=2\pi/\lambda$ is the wave number of the sinusoidal imperfection. Imagine also that an incoming wave of the form,

$$A = exp\{-i(\omega t - k_z z)\}$$

is going to hit the surface and be reflected back. The scattered part of the wave will have a form described by the sum of the two wave contributions,

$$B = exp\{-i(\omega t + k_z z)\}\, a \sin(k_x x) = 2a\, exp\{-i(\omega t + k_z z + k_x x)\} - 2a\, exp\{-i(\omega t + k_z z - k_x x)\}$$

This means that the scattered wave consists in two waves with different directions on the x-z plane.

By these simple calculations it is possible to find that the scattered angle θ is related to the ratio between the wavelengths that characterize both the laser wave and the mirror surface,

$$\tan(\theta) = k_x/k_z = \lambda_z/\lambda_x$$

Of course, this is only the most simple case of waveform surface imperfection for the mirror and actually a real mirror must be described by an infinite number of contributions at different wavelengths. For example, suppose that our mirror surface is made up the sum of n distinct waveforms and that it can be expressed in the following way,

$$S = \Sigma_n a_n \sin(k_{xn} x)$$

In real life we can perform a Fourier transform of the actual mirror surface and consider each Fourier term as a separate scattering surface wave. Then we can try to extract each different contributions from the Power Spectral Density (PSD, Fig. 2) which describes how the power of a signal is distributed with frequency [1], and which is strictly related to the BRDF (Bidirectional Reflectance Distribution Function) of the mirror surface. This last function is the most important tool when we are working with surface roughness and it describes the ratio of reflected radiance exiting from a surface in a particular direction to the irradiance incident on the surface from another direction. Thus, from these considerations we know that by integrating the BRDF over the solid angle we can obtain an estimation of the energy lost.

Also, and more importantly, if we know exactly the BRDF, we can reconstruct, by inverse Fourier transform, the topography of the mirror's error figure. We cannot know the complete BRDF because the Laser beam illuminates the mirrors only from the perpendicular direction. Even a rough knowledge of the BRDF can give us important clues on the characteristics of the mirror deviations from its exact profile, and point to the source of losses. Monitoring the BRDF changes over time would signal the appearance of scattering defects and tell us about their nature. For example the appearance of scatter light diffused over large angles would indicate the appearance of point scatterers, and possibly their average size. This would point to dust and particulate problems. The appearance of scatter at very small angle would indicate low frequency warping of the mirror surface generated by localized non-uniform absorption. This may point to evaporative problems.

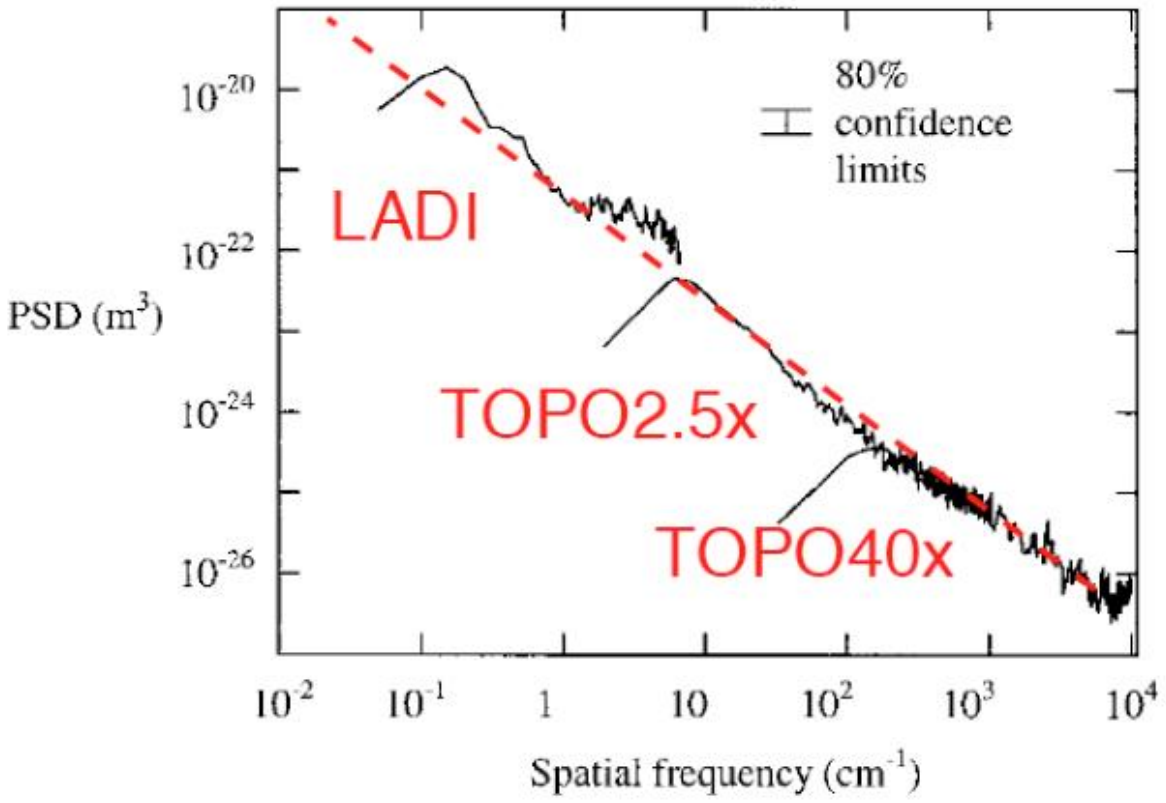

Figure 2: Estimated PSD function for the ITM. This is Fig. 1 in reference [1].

Taking into account of these mathematical tools, it is possible to distinguish the different contribution of the total scattered light and connect the detected power distribution in an array of positions along the interferometer arm to the typical surface contribution, which has produced that scattering.

The present feasibility study of a scatterometer able to work in vacuum conditions, consists mainly in evaluating some of the difficulties in putting photodetectors in different positions inside the chamber containing the main laser beam.

The work can be divided into two main steps:

- an electronic study of the working features of the detectors that may be used in the project and an understanding of its limitations; we propose to use UHV compatible diodes similar to those used for the main interferometer signal detection,
- a geometrical study of the arm chamber in order to understand the best positioning to gather the most interesting information from the scattered photons.

Photodiode calibration

As in every experiment it is extremely important to know the characteristics of the detectors and, in the case of photodetectors, how they respond to an incident light power and what is their power level.

The system used to perform the first calibration stage is made of two different circuit electrically separated: LED-system (LED, Light Emitting Diode, Fig. 3) and PD-system (PD, Photo Diode, Fig. 4).

The LED-system consists of an LED, a load resistance R_L, connected in series to the LED to control the current and to safe it from extra currents able to damage it, and a switch.

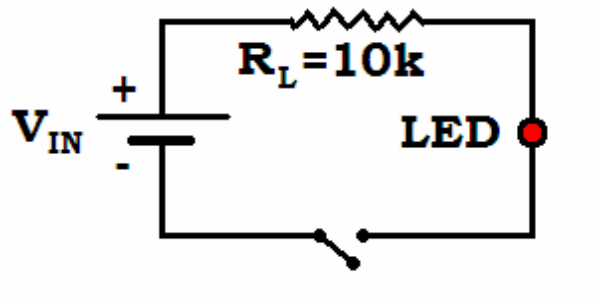

Figure 3: Scheme of the LED-system.

The PD-system consists of a PD and a resistance R_P, connected in parallel in order to amplify the output voltage from the PD. Two or three PD were considered in this study. The PD is the Ultra High Vacuum compatible, and could be used inside the LIGO vacuum.

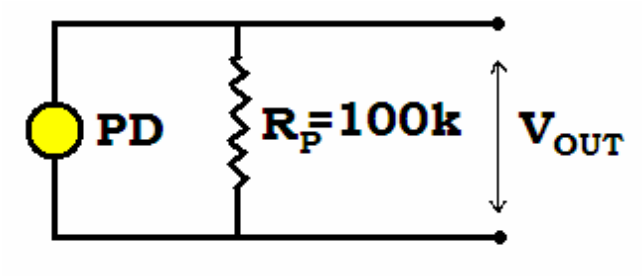

Figure 4: Scheme of the photodiode's circuit.

The PD can be considered as a simple current generator, which causes a photocurrent proportional to the amount of the absorbed light, to run through the resistance R_P. By Ohm's law, the voltage V_{out} (PD) measured across the R_P is proportional to the current (I) and the resistance (R_P), larger resistance makes larger output voltage; in other words the resistance R_P determines the "amplification" of the signal from the diode.

The two most serious drawbacks of this circuit are that it slows the response of the PD and decreases the voltage range over which it has a linear response. As a matter of fact, the PD has an inherent capacitance, so this circuit is essentially an RC filter, and as R_P increased, the RC time constant increases as well.

When measuring the change of a signal over time, the signal must not change faster than the circuit will respond. Biasing the PD would increase the depleted region in the diode and drastically reduce its parasitic capacitance, thus acceleration the response, but it would also increase the dark current, which may be time and temperature dependent. Since changes of scattering are expected to be quasi-static effects, and the stored beam power is as stable with time as possible, response speed is not a consideration in a scatterometer, and only a PD in photocell mode was considered.

To maintain linearity in photocell mode the signal must be very small compared with the band gap voltage, if we want a diode to be sensitive to low light powers, we should use a large resistance, knowing that the response won't be linear with incident power for bright beams; if the photocurrent over the load resistance is sufficiently high to produce a significant voltage drop (as compared with the band gap voltage), charge recombination ensues, destroying a fraction of the signal growing with increasing voltage drops. If we want a linear response in regions of larger illuminance, we may need to use a lower resistance. In all cases it is our interest to maintain the PD in a very low voltage regime while using the highest resistance compatible with that regime, and use a sensitive instrument to measure the output voltage.

In order to characterize the PD-system, I generated a periodic signal as input to the LED-system and measured the output signal through a spectrum analyzer. The use of the spectrum analyzer is dictated by the necessity of being aware of which are the most important sources of noise around

the system. My measurements have been performed for different resistances R_P (0.1, 1, 10 and 100 kOhm) at 100 Hz and 1 kHz frequencies, respectively (Fig. 5).

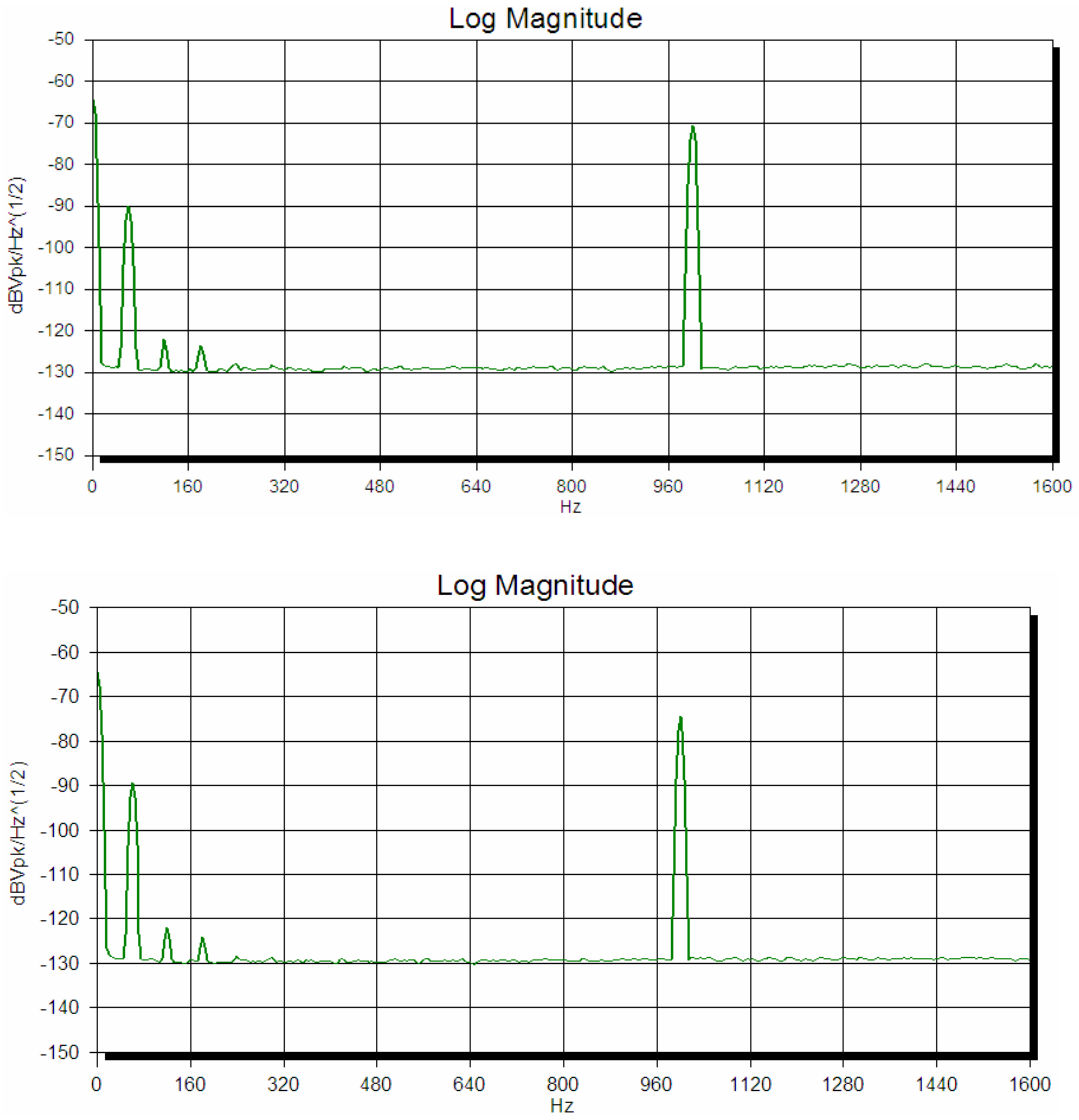

Figure 5: Output signals from the photodiode measured by a spectrum analyzer. The upper graph shows the signal spectrum when the LED-system is in ON configuration with the peak of the signal centred at 1 kHz, as expected. The lower spectrum shows the signal spectrum when the LED-system is in OFF configuration. We can still see the peak of the 1 kHz

oscillator, but at lower amplitude. The value of R_P in this figure is 100 KOhm. The low-frequency peaks are the 60 Hz harmonics. Clearly, the residual 1 kHz signal, as well as the 60 Hz harmonics feed through antenna effects in the cabling and diode arrangement.

Measurements have been made both with the switch of the LED-system off and with the switch on, i.e. LED OFF or LED ON.

In LED ON configuration we find the signal at the expected frequency increasing proportionally to the resistance R_P. In LED OFF configuration we find a similar behaviour but with lower amplitude, which means that the output voltage generated by the PD is lower, but it is not zero. This occurs because the PD behaves also like an antenna which is able to catch the electromagnetic radiation generated by the LED driver.

In order to measure the Responsivity of the PD, which is defined by the ratio of the generated photocurrent to incident light power (or equivalently as a *quantum efficiency*, i.e. the ratio of the number of photogenerated carriers to incident photons), I've used the system described above, but in DC mode.

This calibration consists in a direct measurement of the output voltage from the PD (or equivalently the output current) as a function of the input voltage of the LED-system.

I don't need a periodic input signal, but simply a direct current signal (DC). This eliminates the antenna problem, which would have greatly hampered, if not impeded, the measurement at low light levels. The input voltage is generated by a power supply, which allows us to change the input voltage keeping good stability. The downside of a DC measurement is that it is open to different kinds perturbations, first of which is the thermal variation between the ON and the OFF state.

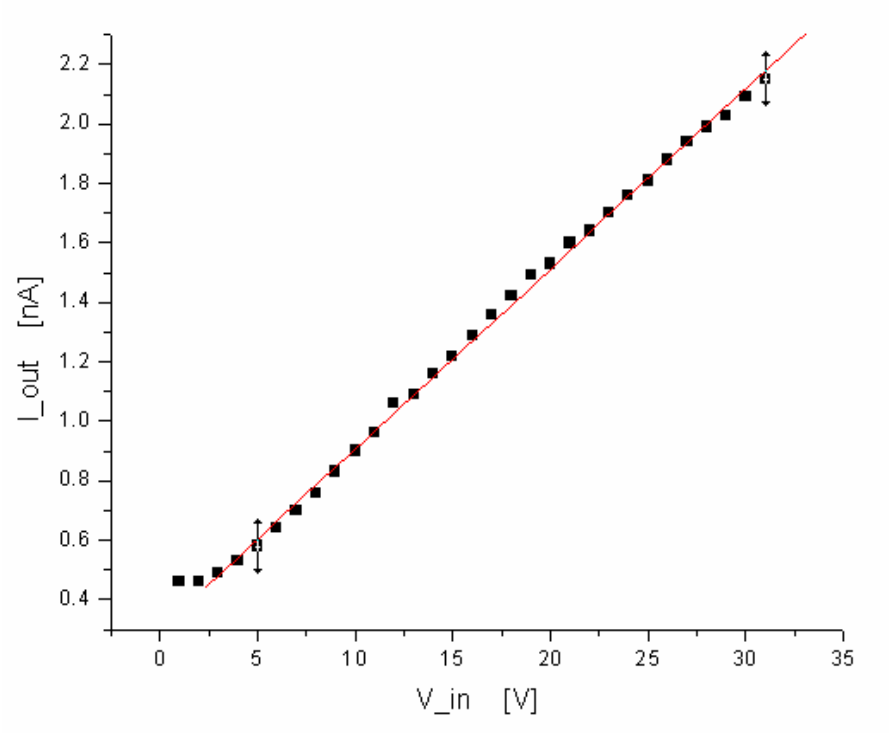

Figure 6: The plot shows the linearity of the photodiode response.

The results of Fig. 6 show that the relation is linear, as we would have expected with such a low current, which means that the responsivity of the PD is constant with the input power. The result of the fit is

$$I_{out}\,[nA] = 0.06\,V_{in}\,[V] + 0.30$$

Another result from this first measurement is the evidence of the temperature dependence of the LED response.

I've measured the output voltage just after turning from the switch off to the switch on configuration and I've repeated this measurement during time in order to record all the variations of the output voltage until its stabilization. The measurement (Fig. 7) has been also performed by making subsequent transitions between low input voltage configuration and high voltage one and vice versa.

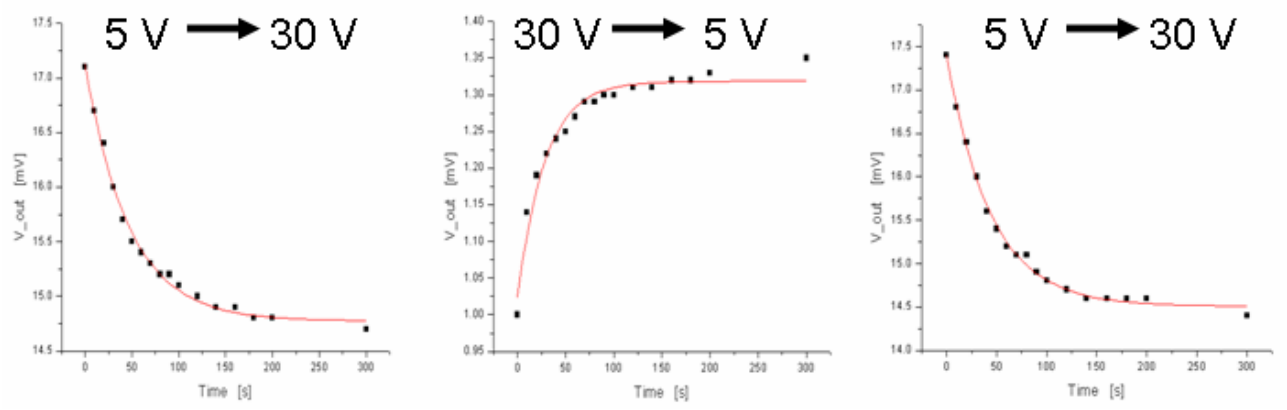

Figure 7: Study of the behaviour of the output voltage of the photodiode during time. The upper voltages show the transition performed.

The fit of the data points, using a 1st order exponential decay, are

$$V_{out} = 14.8 - 2.3 \exp\{-(t/47)\}$$

$$V_{out} = 1.3 - 0.3 \exp\{-(t/28)\}$$

$$V_{out} = 14.5 - 2.9\ exp\{-(t/44)\}$$

The clear result obtained is that the responsivity of the LED change with the temperature and more exactly it decreases with increasing temperature with a time constant of the order of the minute, well compatible with the heating time of the LED case.

In order to avoid this problem in the system the LED should stay in ON configuration for all the measurements period without changing the LED power, which makes it varying its temperature. So the attenuation of the LED light can be made using a system which allows to block totally or partially the photons from the LED to the PD. This system is a particularity of the second configuration described later. In Fig. 8, I show how the attenuation is not difficult to obtain

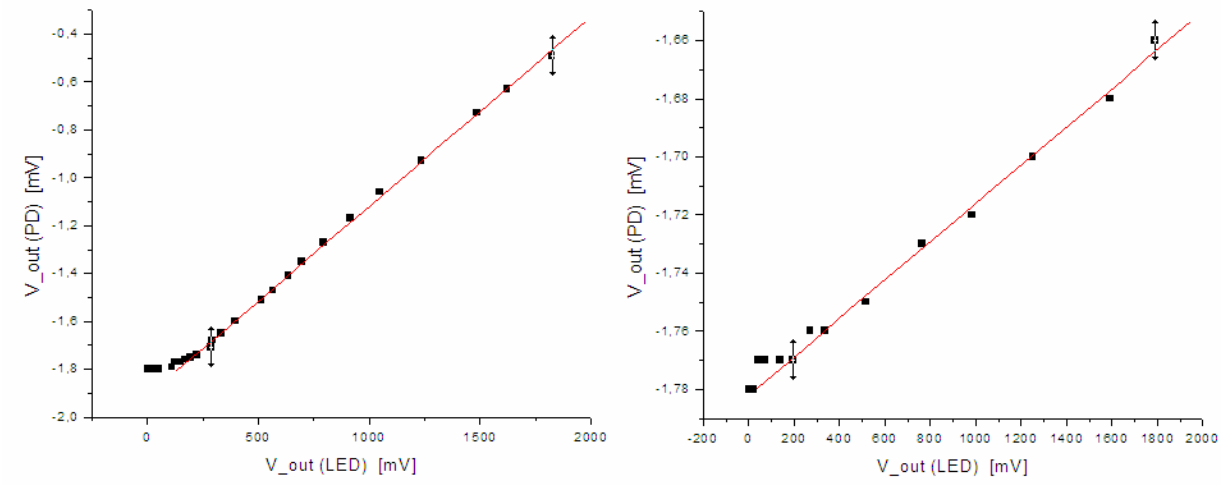

Figure 8: The plots show two attenuation stages, where the right one refers to an attenuation 7 order of magnitude greater than the left one. The plots recall the configuration explained in the following pages.

The results of the fit give

$$V_{out}(P)\ [mV] = 8.0\ 10^{-4}\ V_{out}(L)\ [mV] - 1.9$$

$$V_{out}(P)\ [mV] = 6.6\ 10^{-5}\ V_{out}(L)\ [mV] - 1.8$$

From all this first measurements, it has been possible to realize that most of the background noise which affects the PD is coming from the wiring system, which it is very clear by looking at the measurements with the spectrum analyzer. In fact, it is easy to recognize in the spectrum the component at 60 Hz together with all its higher harmonics (see Fig. 5).

In order to reduce this source of noise the first step is to avoid any electrical connection to the wiring system and for this purpose I've made some modifications to the system configuration.

The photodetector employed for the measurement in the new configuration is different from the previous one being more suitable to the vacuum condition responding to the low noise requirement. It is a large area InGaAs photodiode, model C30642, which yields high responsivity from 850 nm to 1550 nm and low dark current (Fig. 9, 26).

Figure 9: Picture of the InGaAs photodiode model C30642. The datasheet of this photodiode is available at http://www.ortodoxism.ro/datasheets/perkinelmer/C30665.pdf.

The collected noise also reduces with lower photodiode parallel resistance R_P, lower resistance will also reduce the signal amplitude. The best choice of R_P to maximize the signal to noise ratio will depend on the illuminance level.

First I physically separated the PD-system and the LED-system isolating them in different boxes and connected them through an optical fibre.

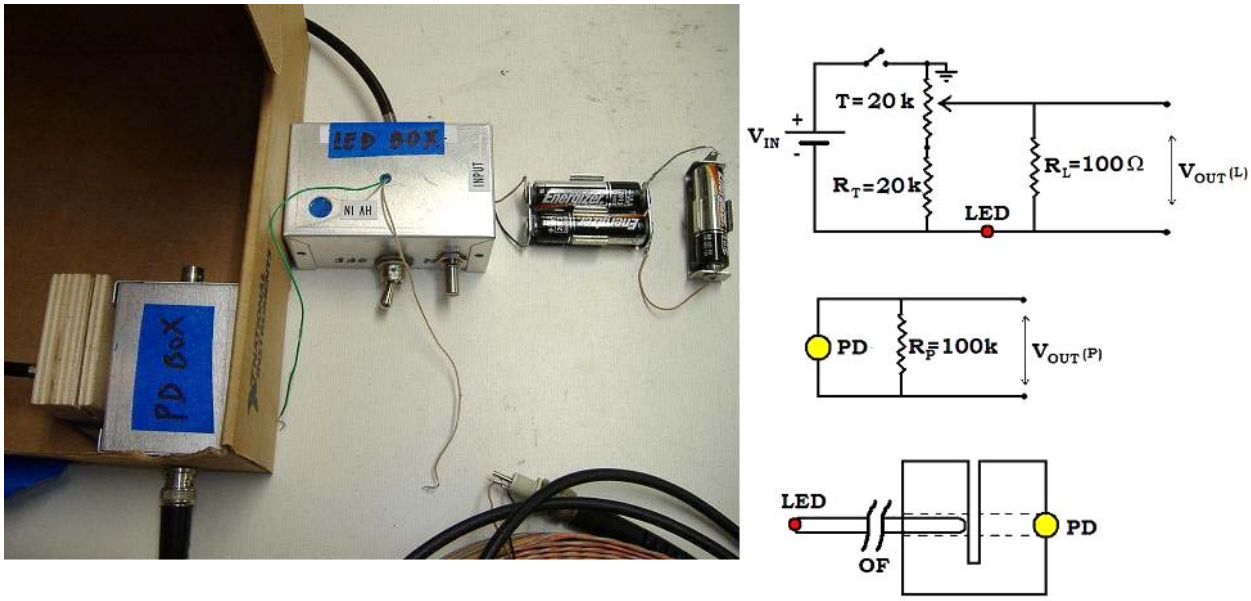

Figure 10: Picture and schematic view of the working configuration. (right from top) LED-system, PD-system and system used to connect the optical fibre to the systems.

The connection system (Fig. 10) is made up a cube of wood in which I drilled a through hole to fit the PD in one side and the optical fibre from the LED in the other. I made a slot in the block to allow the introduction of a shutter between the PD and the LED fibre. The slot can be also used to insert an attenuator to reduce the transmission of the LED light without changing its current. Using the shutter instead of switching on and off the LED circuit eliminates the LED heating problem.

The second, less important, modification is the use of a simple battery as a replacement for the power supply. In this way some of the electrical noise caused by the wiring system is eliminated.

Introducing a battery we lost the opportunity to change the input voltage directly acting on the power supply. To tune the light output, I've added a 20 kOhm range potentiometer in series, to change the current running through the LED.

In this case the current running through the LED, which is proportional to the ratio of the input voltage (constant) and the resistance (varying), change proportionally to the inverse of the resistance (Fig. 11).

Since we expect a linear response of the PD to the photons from the LED, the same trend should be found for the output current of the PD.

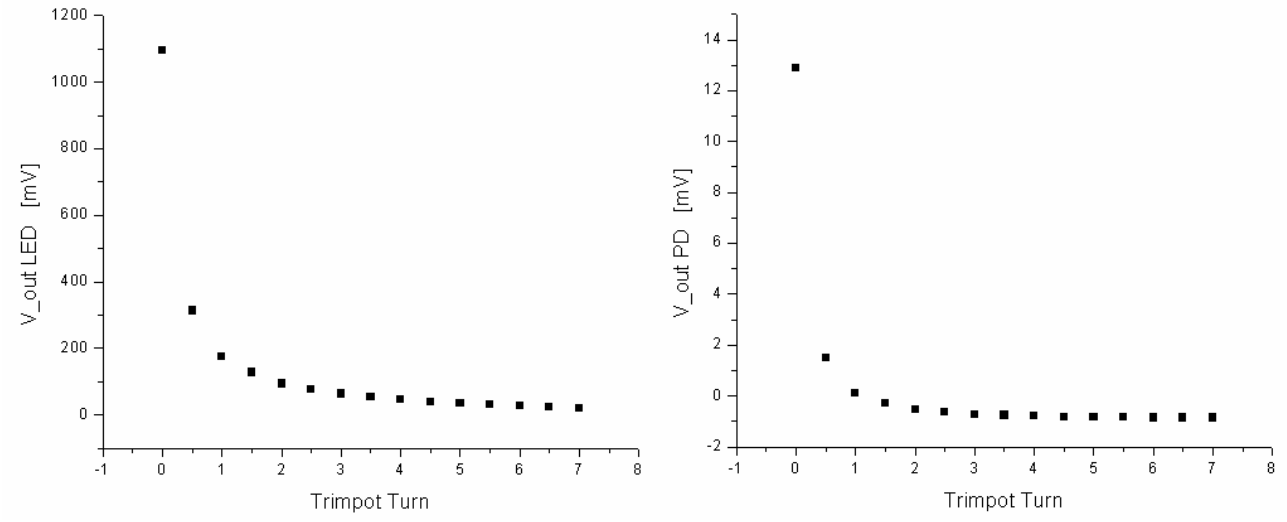

Figure 11: The two plots show the expected trend of the output voltage (output current) as a function of the changing resistance provided by the trimmer. In the abscissas, the units are expressed as ¼ of turn, which is strictly connected to the resistance.

As a cross check, we plotted the output voltage of the PD as a function of the voltage of the resistance R_L in series with the LED, finding the expected linear behaviour (Fig. 12).

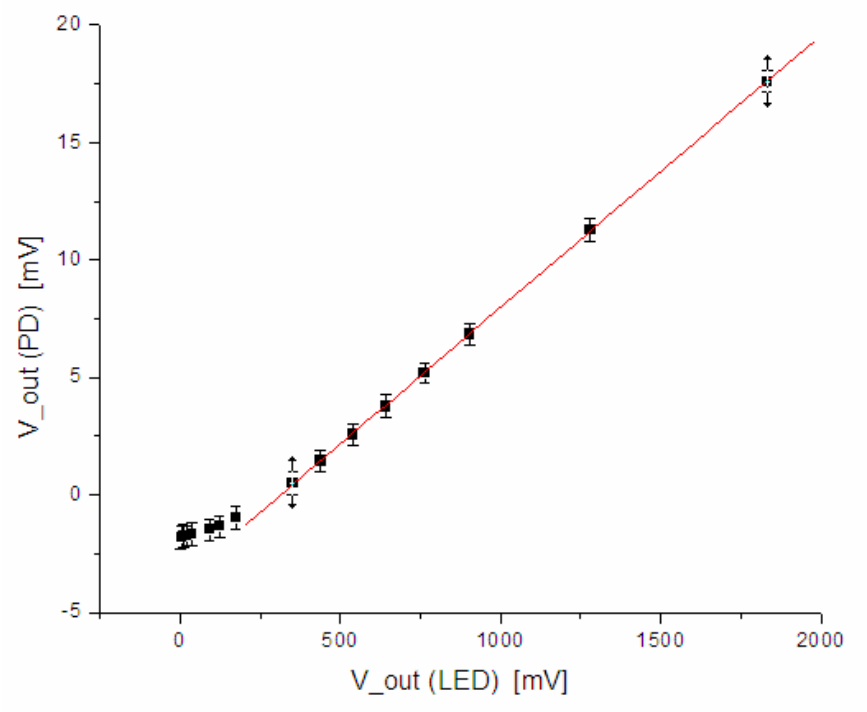

Figure 12: The plot shows the linearity of the photodiode response. The error bars emphasize the measured noise which will be discussed subsequently.

The fit result gives,

$$V_{out}(P)\ [mV] = 0.012\ V_{out}(L)\ [mV] - 3.6$$

where the *3.6* mV deviation from linearity is attributed to parasite resistance in parallel to the LED.

In addition to the linear response of the photodiode, another measurement can be performed in order to understand how the photodetector responds at an high intensity input power . In fact, if the intensity of light is too great on the surface of the photodiode, it will saturate. This occurs when

there are far more photons reaching the diode than there are available electrons that can be excited. When this happens, the diode will no longer have a linear response. In order to increase the input light coming from the LED, I've changed the input voltage replacing a battery of about 17 V instead of the previous 4.5 V, and the above described effect is clear in the Fig. 13.

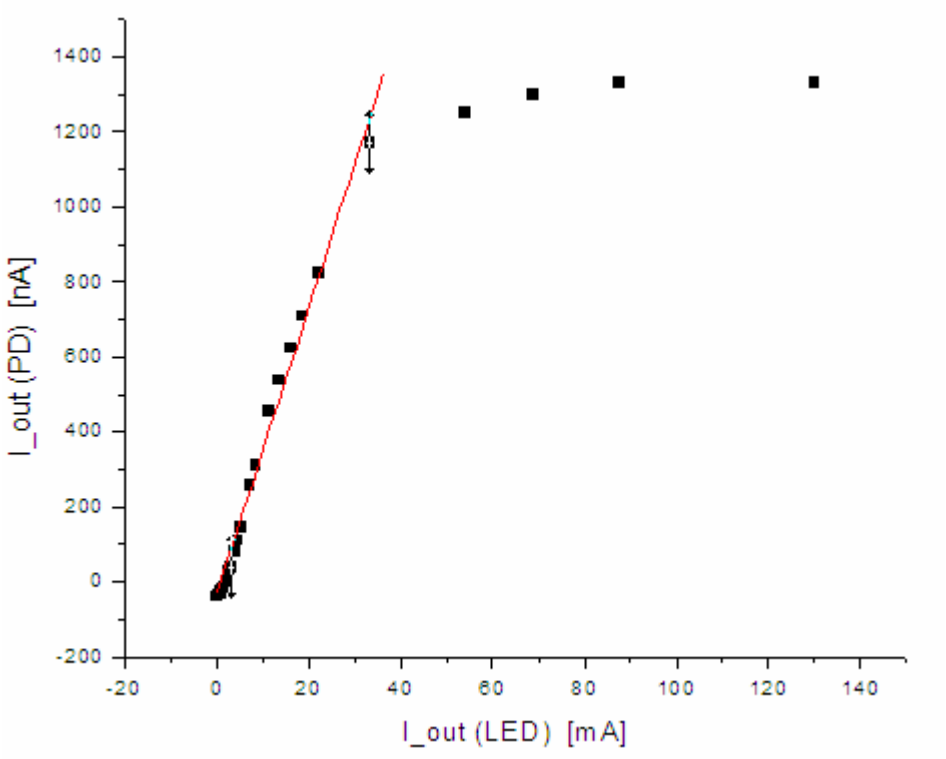

Figure 13: In the plot it can be noted that the system doesn't respond linearly any more with a current greater than 1 μA running in the photodiode. For our purpose it is necessary to work far away from this region and to focalize in the linear range response. Although the presence of the saturation effect, in this plot the linear range is also evident.

The saturation has been reached after changing the R_L resistance in parallel to the photodiode (100kOhm) with a greater one (1 MOhm) so that the signal produced in output would be larger.

The result of the fit is

$$V_{out}(P)\ [mV] = 0.05\ V_{out}(L)\ [mV] - 9.1$$

This measurement is important for two reasons: to understand at which level of input power it is necessary to mount a smaller resistance in parallel to the photodetector in great intensity light regions, and to make sure if it is important or not to use a lens before the photodiode to collect more photons without reaching the detector overfilling.

Since the purpose of the study is the feasibility of an in vacuum scatterometer, I need to operate the photodiodes as close as possible to the vacuum conditions. Since active components in vacuum are risky I study the possibility to amplify the photodetectors signal only outside the vacuum chamber. To do this, it is necessary to lead the output signal from the photodiodes (inside vacuum) to the amplifier (outside) through cables, preferably twisted pair (to minimize induction or antenna effects). The amplifier used for the measurements is a D070254 Dual-Channel, Externally-powered Low Noise Preamplifier shown in Fig. 14.

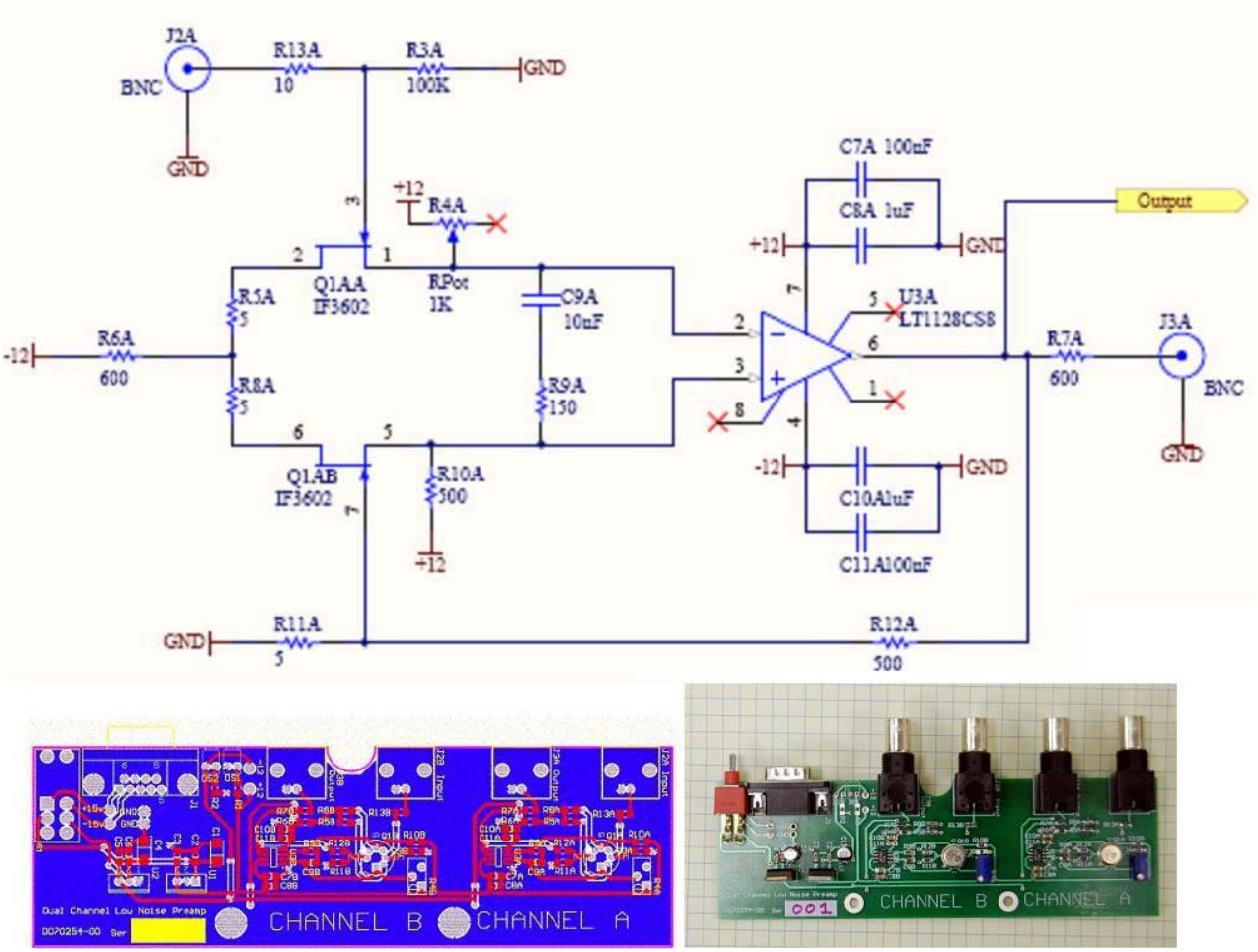

Figure 14: The upper figure shows the electric scheme of the amplifier (only one of the two channels), the gain is set by the ratio between the resistance R12 and R11 which is about 100. In the bottom are shown the board scheme (left) and the picture of the amplifier (right).

Although there are two available channels, I used only one of them for my purpose. The amplifier gain is set by the ratio between the R12 and R11 resistances (see Fig. 14)

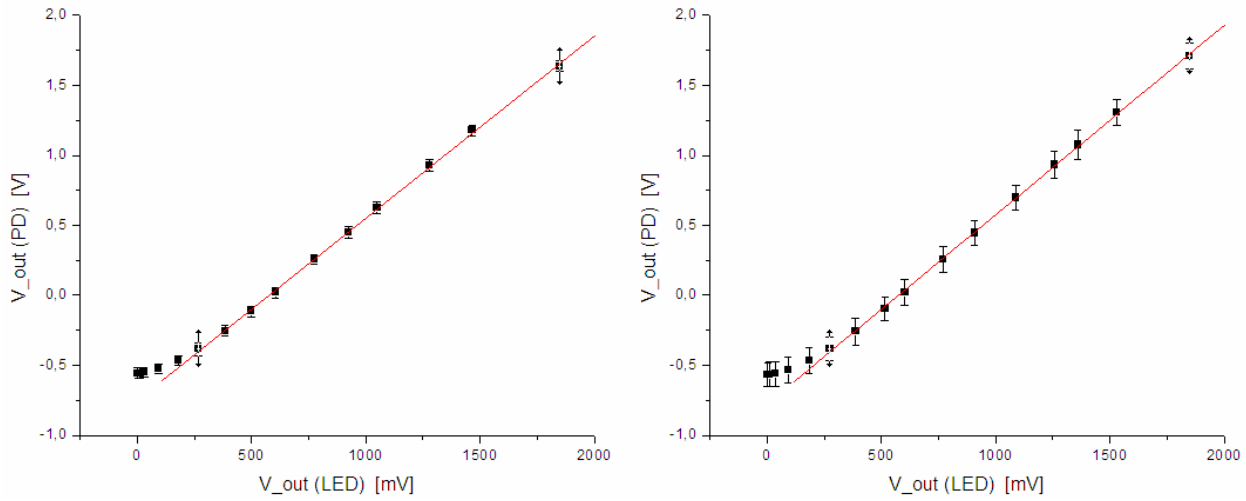

Figure 15: The plot shows the linearity of the photodiode response amplifying the output signal locally (left) and connecting to the amplifier via 10m of twisted pair cable (right). Note the expected increase of the noise between the two measurements.

The gain and offset results are independent of the cable presence (Fig. 15):

$V_{out}(P)\ [V] = 1.30\ V_{out}(L)\ [V] - 0.75$ *amplifier*

$V_{out}(P)\ [V] = 1.37\ V_{out}(L)\ [V] - 0.79$ *amplifier + cable totally twisted*

$V_{out}(P)\ [V] = 1.35\ V_{out}(L)\ [V] - 0.78$ *amplifier + cable not twisted at the two ends*

However, the important feature to characterize the scatterometer is the noise produced by the photodiodes with and without cables.

Noise calibration

The noise has different origins: shot noise (photons contribution), background noise Y (wiring system) and the dark current X (the current through the photodetectors in absence of light), light generation noise, and other unidentified sources,

$$N^2 = X^2 + Y^2 + g^2 n_f$$

where g is the quantum efficiency of the photodiode and n_f represents the number of photons.

If there weren't instrumental noise, we should measure shot noise linear with the square root of light intensity, except for very low input voltage for which the dark current noise would dominate.

From a first measurement with high light level we can in principle estimate the total noise, i.e. the noise due to the sum of the three contributions. From a second measurement, using something to block the photons from the LED (shutter), we can estimate the noise due only to the dark current of the PD and to the background noise.

By subtracting the second measurement from the first one, we estimate the noise only coming from the photons (shot noise and light generation noise).

Then, since we know the quantum efficiency (g) of the photodiode (from its datasheet) if we assume that the noise measured is shot noise, we can calculate that the shot noise is g multiplied the square root of the number of photons (n_f) caught by the PD and we can give an estimation of this

number. This is important because it tells us how many photons, for a given input voltage, the PD catch and what is its response.

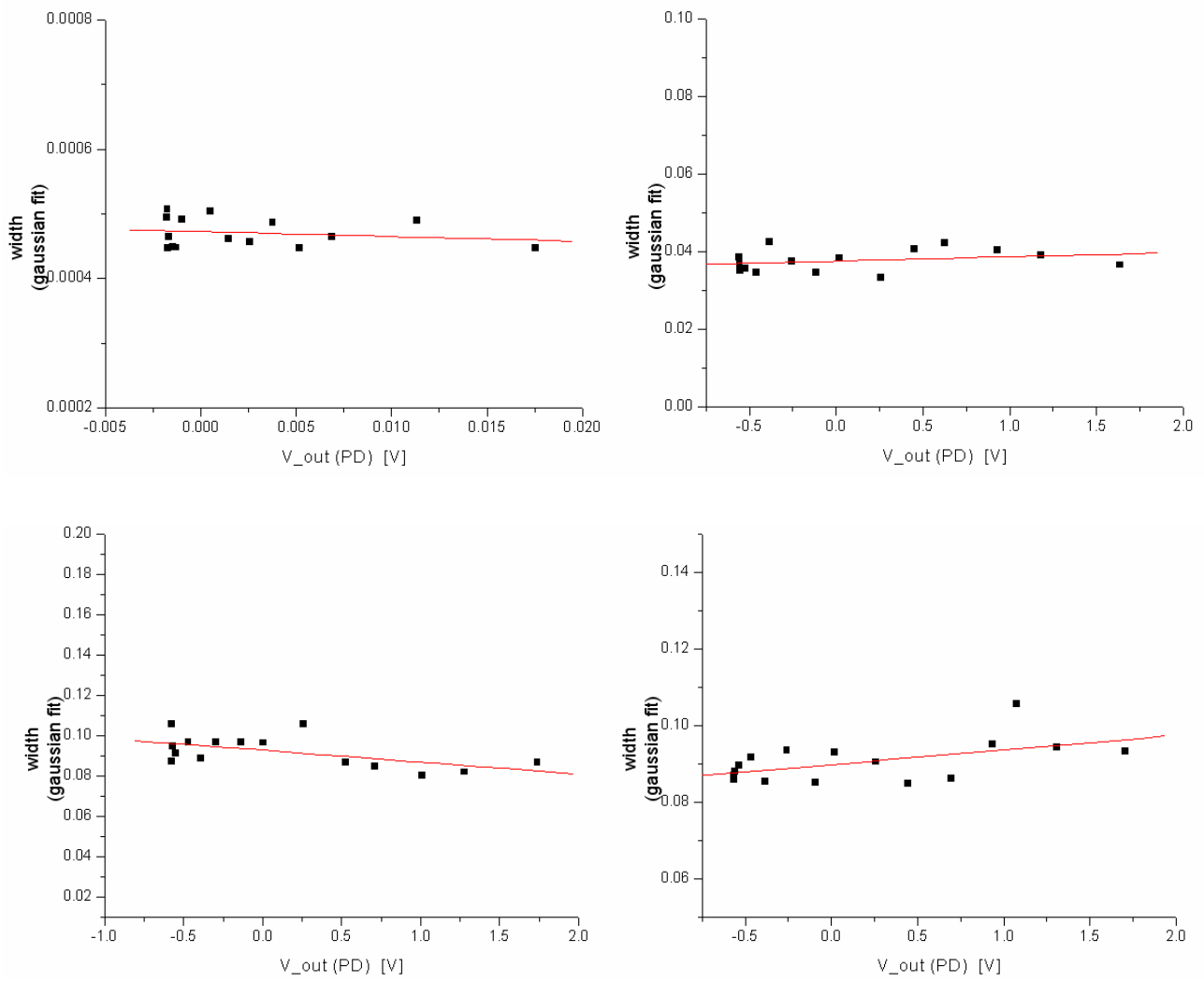

Figure 16: The plots show the change of width of the gaussian profile of the noise measurement for different output voltage of current levels into the photodiode. (top left) Direct measurement of the output voltage, (top right) amplified output, (bottom left) amplified output using a twisted pair cable to connect the system to the amplifier, (bottom right) the cable is not totally twisted at the two ends.

I performed this measurement for different output voltage (LED or PD) to find a connection between the input voltage (i.e. the current through the LED) and the noise produced by the PD. From this noise analysis we can see that the noise increases when we put the system amplifier plus cable after the PD.

The noise level present with the only PD (Fig. 16), amount to

$$\sigma_m = 0.47\ mV$$

where σ_m is the mean value of the measured gaussian width and which takes account the contributions from the dark current of the photodiode (intrinsic noise), the noise from the BNC cables and that from the wiring system which, even if it is attenuated, is not totally eliminated.

The noise level measured when we amplify the output signal is much greater and it amount to

$$\sigma_m = 37.8\ mV$$

The noise measured with the amplifier plus the twisted pair cable is

$$\sigma_m = 92.1\ mV$$ *totally twisted pair cable*

σ_m = **90.6 mV** *the cable is not twisted at the ends.*

What we observe is, as expected, an increase of the noise of the photodiode's response when we increase the output voltage and much more when we connect the output of the photodiode to the amplifier through a twisted pair cable.

Instead, we don't observe a increasing noise for increasing input current. In fact from the results of the fits of the width from the noise gaussian fits, we note that the data points are distributed in a casual way. This means that the shot noise of the photons is overpowered by the instrumentation noise which.

A better way to measure the noise level of the system is checking how the system responds at frequencies of interest (lower than 100 Hz). The reason of working at very low frequencies is dictated by the necessity of a stability check of the photodiode response which could change in long time intervals. The instrument used to perform these measurements is a spectrum analyzer which I set to measure the frequency range between 0.1 Hz and 100 Hz.

After starting all the measurements, the first step consists in setting the zero noise level of these measurements; I need to know how much noise comes from the spectrum analyzer itself (Fig. 17).

Then I can proceed first in measuring and recording the spectrum generated by the output of the photodiode system. The measured spectrum is shown below, and represents the noise distribution of the whole system (Fig. 18). The same measurement is also performed after amplifying the signal from the PD (Fig. 19) and also using the twisted pair cable to connect them (Fig. 20).

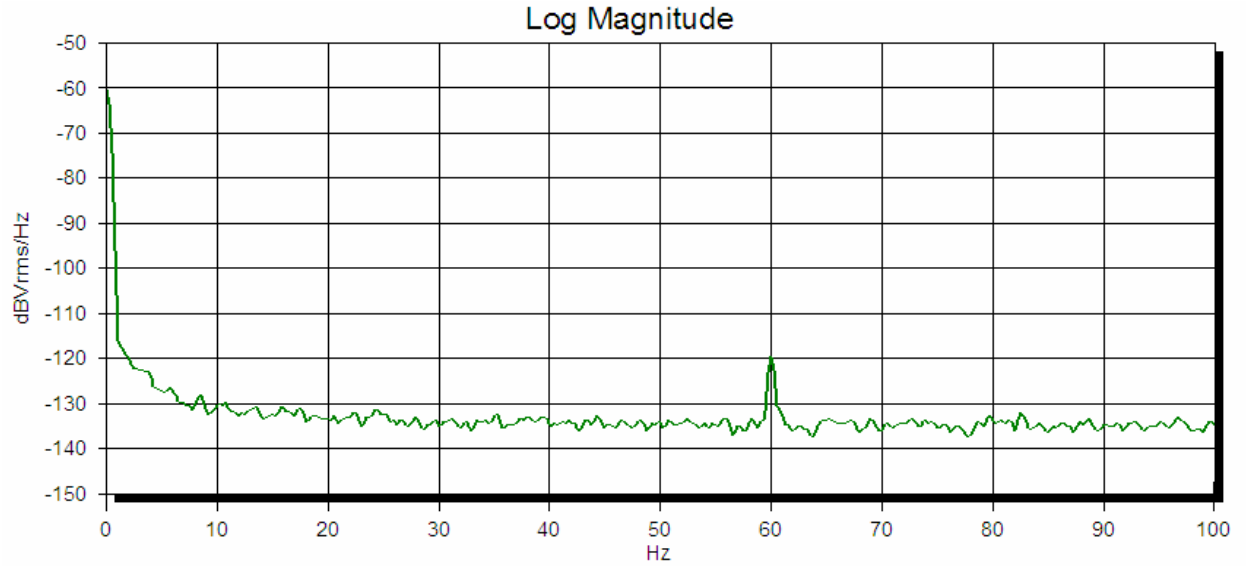

Figure 17: The spectrum generated by the spectrum analyzer itself which, in these measurements, allows to set the zero of the noise system. It can be seen that the effect of the wiring system affects also this instrumentation and will be summed to the other contributions given by the LED-PD system.

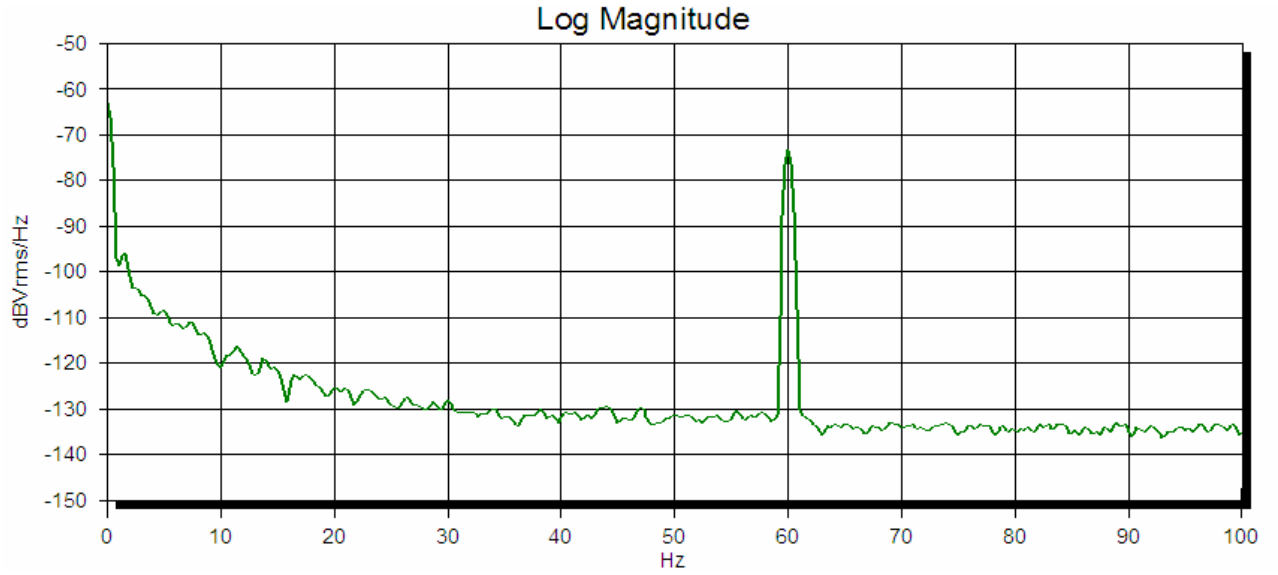

Figure 18: Noise spectra generated by the photodiode signal. The noise dominate at very low frequency, decreasing by about a factor of 30 dB after 30 Hz. The peak centred at 60 Hz is the wiring system first harmonic.

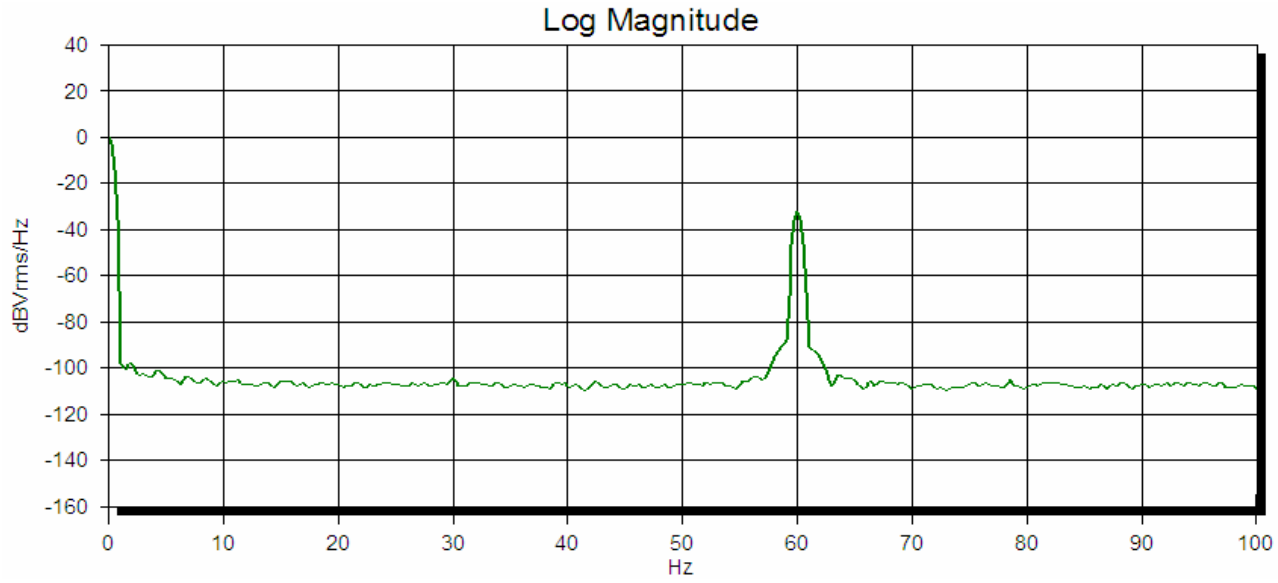

Figure 19: Noise spectra generated by the photodiode signal after its amplification. In the low frequencies range the noise is essentially unchanged but the signal to noise ratio is 100 times

greater, because of the gain of the amplifier. For frequencies greater than 30 Hz the signal to noise ratio is also larger but only by a factor of 10.

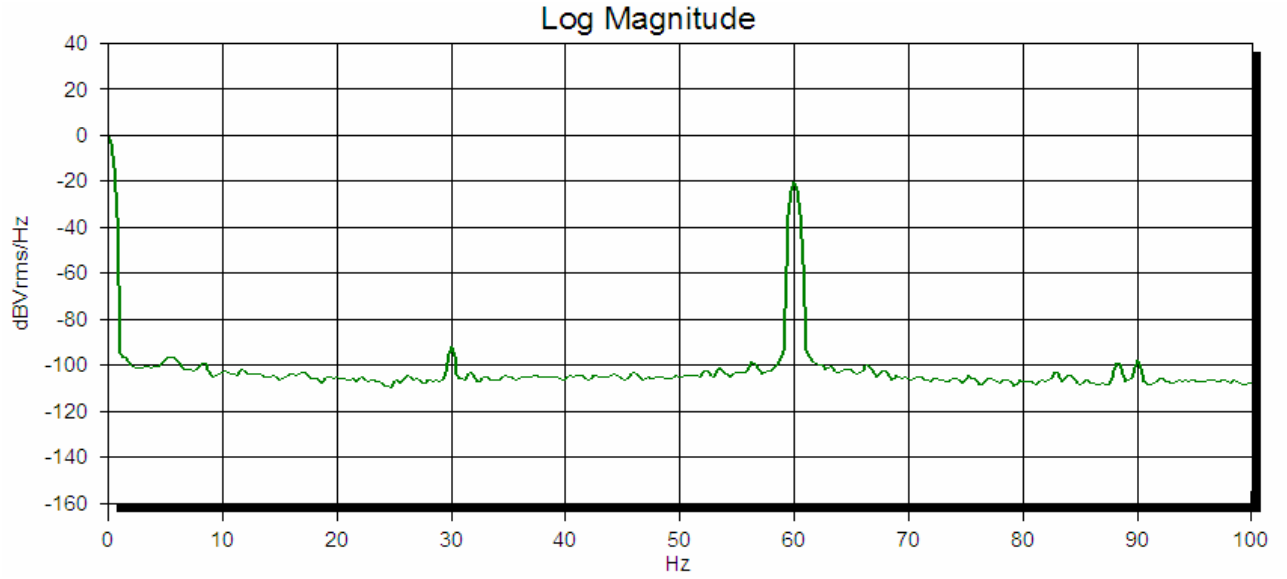

Figure 20: Noise spectra generated by the photodiode signal after its amplification with 10 m of twisted pair cable to lead the signal to the amplifier. The result is almost the same with or without the cable even if the antenna's effects are stronger in this configuration (see the peak at 30 Hz of the first semi-harmonic of the wiring system).

The noises found by integrating over the frequency range are listed in Tab. 1.

System	Voltage (μV)	Current (nA)
spectrum analyzer	2	0,02
photodiode	30	0,30
photodiode with amplifier	35	0,35
photodiode with amplifier and t.p. cable	56	0,56

Table 1: Noise results considering different system configuration.

The second important step is to check if the observed spectrum is a measure of the photo detection circuitry, or if it is produced by noise in the test setup, which is the LED-system used to calibrate the photodiode. I measured the spectrum generated by the output of the LED-system to establish whether its noise is the cause of the spectrum that I see at the output of the PD-system (Fig. 21). The result obtained for in this measurement is

$V_{rms\ (LED)} = 2\ \mu V$ *which corresponds to* $I = 20\ pA$

which is essentially the same coming from the instrumentation used for the measurements (see Table 1).

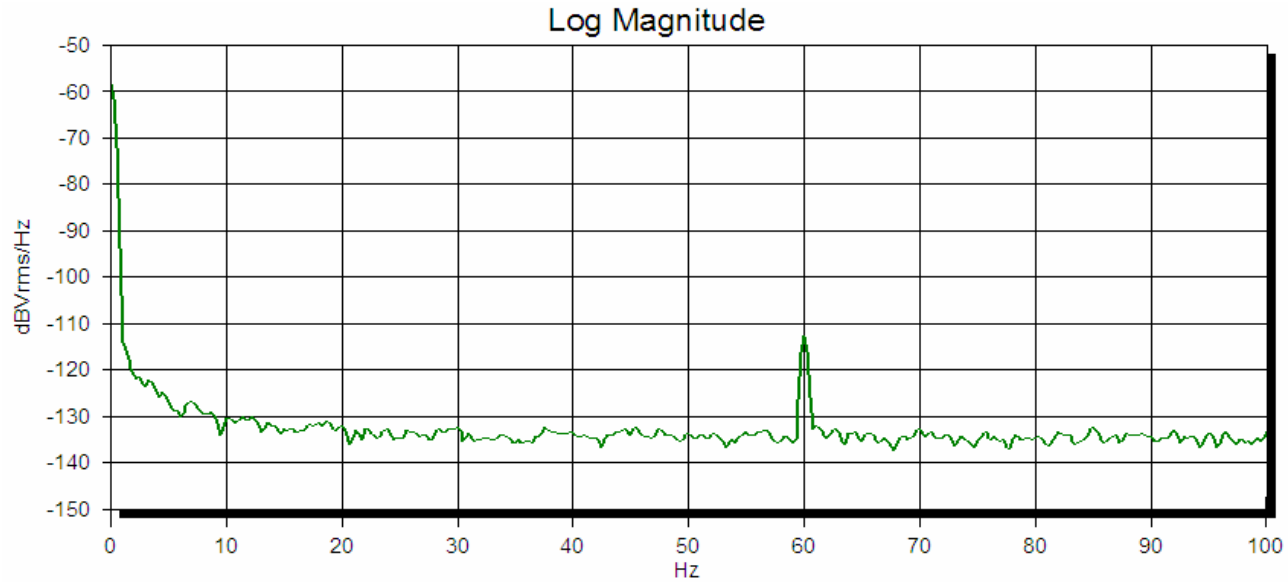

Figure 21: Noise spectra generated by the test setup (LED-system). The noise level observed is essentially the same of that resulting from the spectrum analyzer itself, except for the peak at 60 Hz which is higher because of the antenna's effects introduced by the LED structure.

Moreover, I need to know how the noise at the LED-output is related to the noise at the PD-output, and this is yielded by a simple measure of the transfer function (TF) from the LED to the PD. The easy way for this measurement is to make two different measurements, one from the input of the system to the LED-output and the other from the same input to the PD-output. So that, the measurement of the TF from the two outputs is

$$TF_{OUT(LD)-OUT(PD)} = TF_{IN-OUT(PD)} - TF_{IN-OUT(LED)}$$

Having knowledge of that TF, I can predict what the spectrum at the LED-output will look like at the PD-output (Fig. 22).

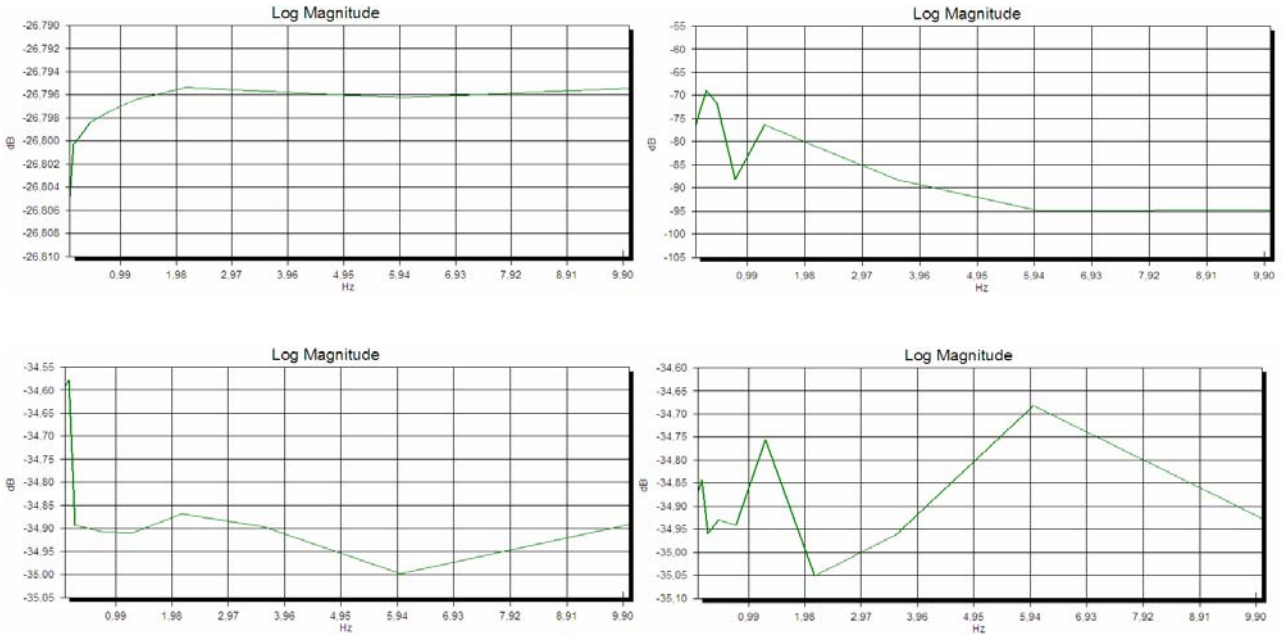

Figure 22: The graphs show the transfer functions (TF) of the system: (top left) the TF between the input of the system and the output from the LED-system; (top right) the TF between the input and the output of the PD-system, which show an increase of the noise level at very low frequencies; (bottom) the TFs between the input and the output from the PD-system with the amplification of the signal (left) and also with the twisted pair cable (right). What it is interesting is the difference between these TF which gives a direct TF from an output to the other.

By integrating the noise equivalent power (NEP) over the frequency range of interest (0 Hz – 100 Hz), I can find an estimation of the noise of the system.

In these measurements I've considered only the noise present in the frequency range between 0.1 Hz and 100 Hz. Most of the noise comes from 60 Hz and above. It will be necessary to provide the scatterometer with a filtering system able to cut off the higher frequencies.

Geometrical study

The aim of this second part of the study consists in inferring the electric current that would be detected by the photodiodes of the scatterometer illuminated by the scattered photons power.

It is important to remark that scatter measurement was already performed in both LIGO sites, but only to estimate the total power losses and to try to separate them into different contributions.

These estimations were performed by two view-ports which allow to look at the ITM from a 45° and 1° directions, respectively (Fig. 23). The choice of these locations for the photodetectors are dictated by the availability of view-ports and the purpose of studying either the wide angle scattered light (45°) due mainly to the point defects on the mirror surface, and the narrow angle scattered light (1°) due to the surface roughness of $\lambda >> 1$ mm. Having only two measurement points, little can be said about the actual shape of the BRDF.

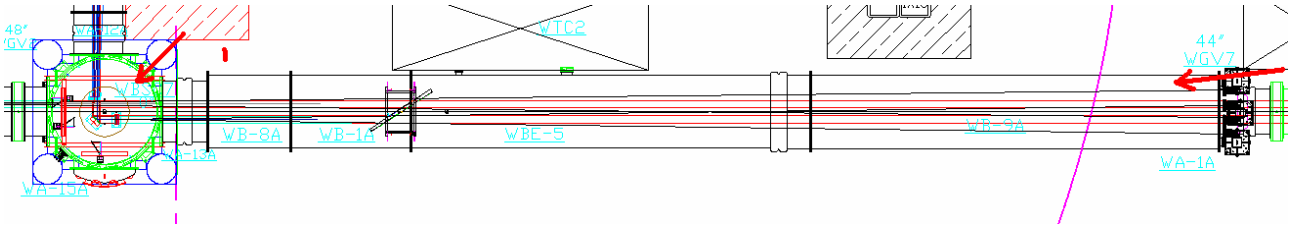

Figure 23: The picture represents the portion of the interferometer between the ITM chamber (right) and the first 30m of the arm. The red arrows indicate the position of the two view ports used in the current experiments led both in Hanford and in Livingston sites. In these measurements the photodetector are located outside the vacuum.

The measured quantity resulting from this experiment is the BRDF of the mirror surface, which gives an estimation of the power lost by the scattering. Having only two measured points, the results are simply used to give provide a scale factor to assumed curves for the BRDF as a function of the scattered angle (θ). The curves assumed to match the experimental points are

$$dP/(P\,d\Omega) = A\,\theta^{-2} \qquad \text{for } \theta < 0.3 \text{ rad} = 17°$$

$$dP/(P\,d\Omega) = B \qquad \text{for } \theta > 17°$$

where the scattered power dP is normalized for the solid angle $d\Omega$ produced by the scattered photons and also for the laser total power P. The constant $A = 6\ 10^{-7}$ and $B = 8\ 10^{-6} / \pi$, are only assumptions based on theoretical arguments and measurements on mirrors outside vacuum. They do not necessarily represent the actual situation in the interferometer.

The trends of these relations are shown in Fig. 24.

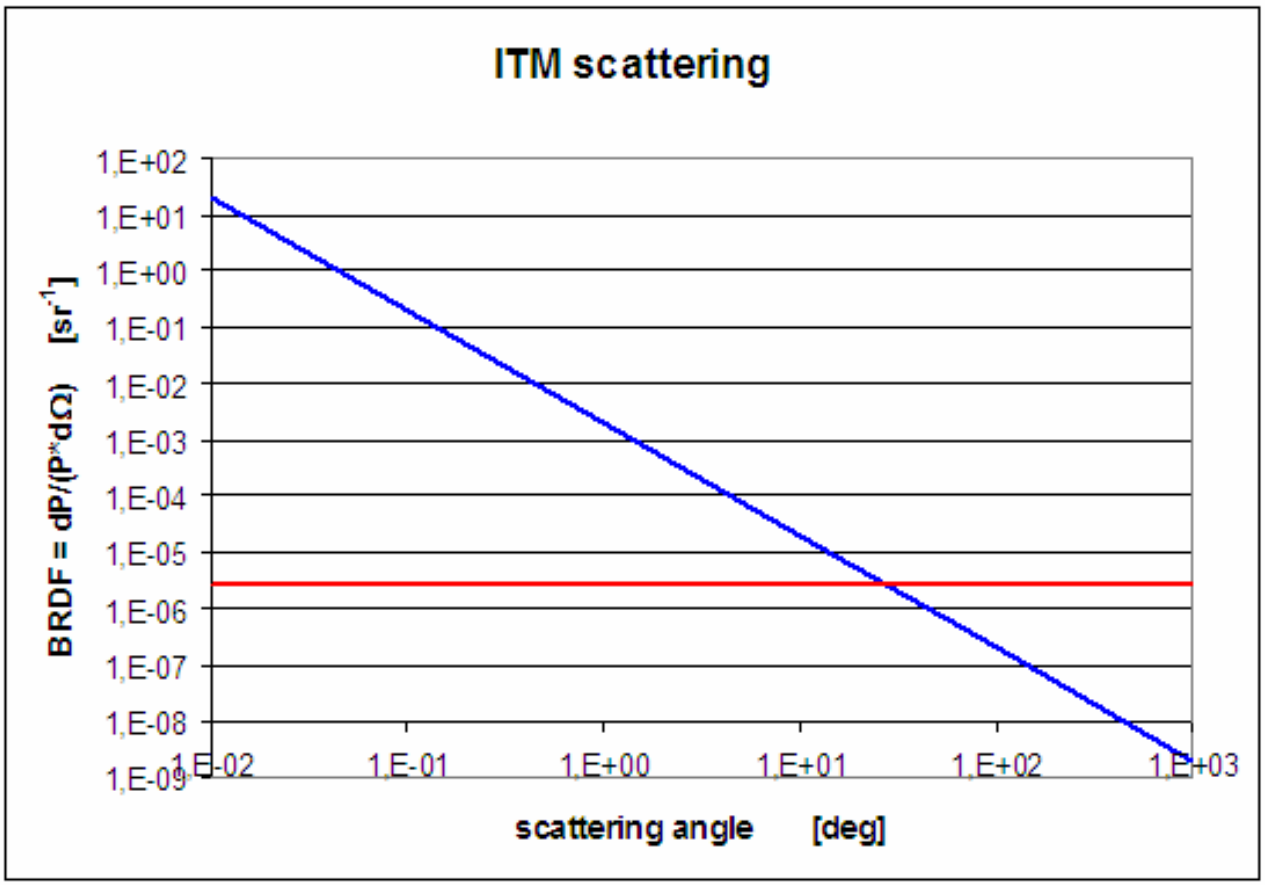

Figure 24: The plots show the relation assumed for describing the BRDF of the mirror (in this case the ITM). The blue trend is used to describe photons scattered at small angles which are due to large wavelength mirror surface imperfections; the flatness assumes a non-structured spectral distribution of these imperfections. The red constant trend is used to describe the effects of point defects on the mirror (inside and outside) which produce an isotropic scattering. It assumes only scatterers with wavelength smaller than 1 μm.

By studying the schematic view of the interferometer (using AUTOCAD), I have been able to extract the geometrical information of the system for a number of proposed detectors positions in

the chamber, their distances from the ITM and the angles between the direction of their line-of-sight to the mirror and that of the main beam (Fig. 25).

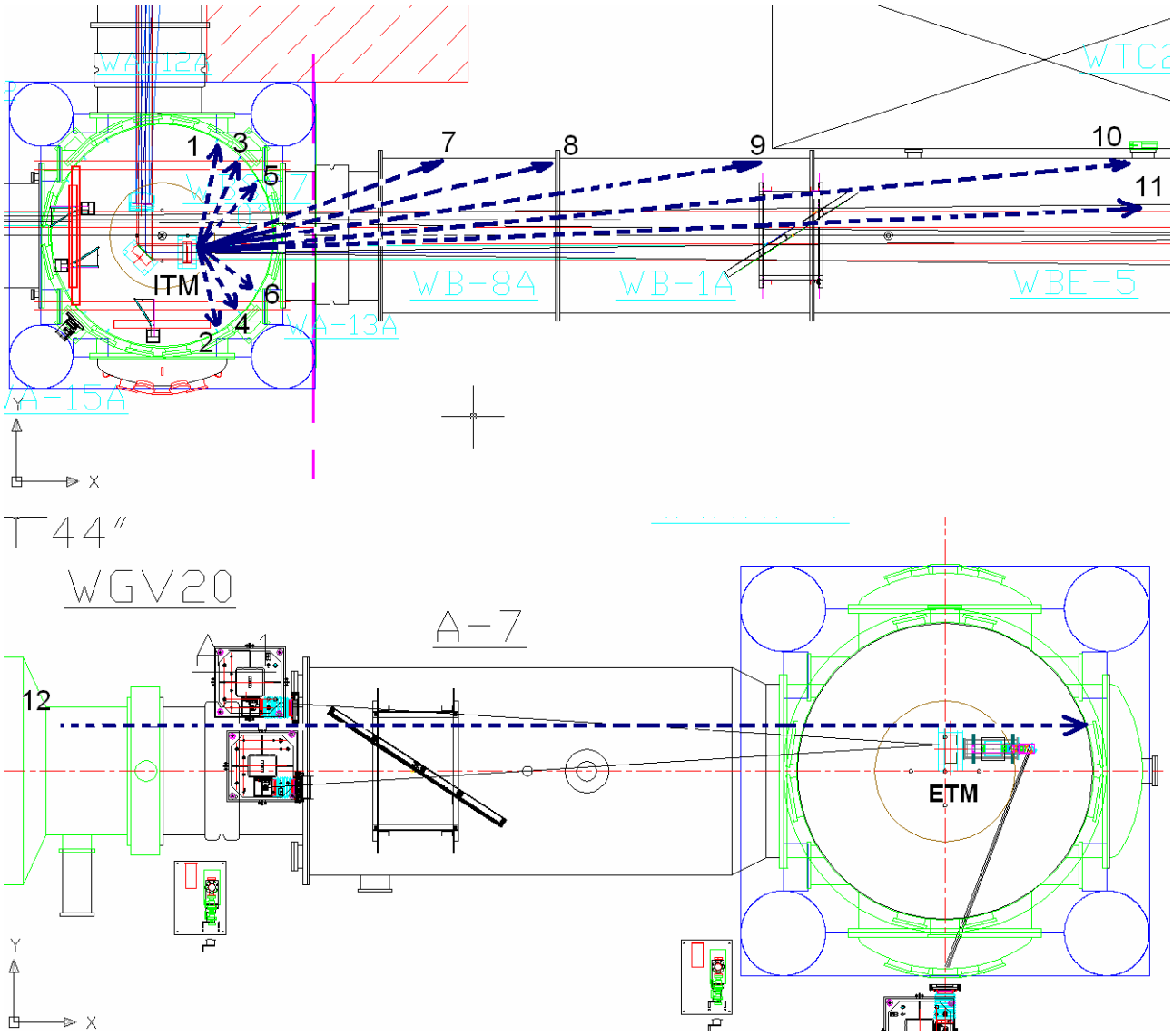

Figure 25: Schematic top view of portion of the interferometer. The upper figure shows the ITM chamber in which it is possible to put the photodetectors using the supports already located at different angles in the chamber (blue dashed arrows) and which would cover the wide angle region. The lower figure represents the scheme of the arm's end at 4 km

(containing the ETM), which can be used to put other photodiodes in order to catch the photons scattered at very small angles. The numbers on the rays refer to Table 2.

After choosing the more useful angles for locating the photodiodes and using the relations mentioned before, I used the assumed BRDF to calculate for each angle the light collected by the PD. The light flux is obtained by multiplying the BRDF by the solid angle, $d\Omega$, covered by the photodiode. This product yields the power of the scattered photons normalized over the laser total power.

The solid angle covered by the photodiode is given by

$$d\Omega = \pi (\theta/2)^2$$

where $\theta = d/r$, and d, r are, respectively, the photodiode's diameter and the distance of the PD from the mirror expressed in mm. Of course we expect to mount the diode perpendicular to its line of sight.

Then, multiplying the dP/P quantity for the laser total power, supposed to amount to 100 kW (actually the design power of the beam stored in the cavity is about 680 kW), obtaining the power which is expected to reach the photodiodes.

All the results are listed in Tab. 2.

ref. Fig. 25	angle (deg)	angle (rad)	brdf (sr^(-1))	d (m)	solid angle (sr)	dp/p	power (W)	current (μA)
1	77	1,34	2,55E-06	1,35	1,72E-06	4,39E-12	4,39E-07	0,31
2	72	1,26	2,55E-06	0,96	3,41E-06	8,68E-12	8,68E-07	0,61
3	63	1,10	2,55E-06	1,24	2,04E-06	5,20E-12	5,20E-07	0,36
4	51	0,89	2,55E-06	0,91	3,82E-06	9,72E-12	9,72E-07	0,68
5	48	0,84	2,55E-06	1,14	2,42E-06	6,16E-12	6,16E-07	0,43
6	30	0,52	2,55E-06	0,89	4,00E-06	1,02E-11	1,02E-06	0,71
7	20	0,35	2,55E-06	2,86	3,84E-07	9,78E-13	9,78E-08	0,07
8	15	0,26	8,75E-06	3,82	2,15E-07	1,88E-12	1,88E-07	0,13
9	10	0,17	1,97E-05	5,73	9,57E-08	1,88E-12	1,88E-07	0,13
10	5	0,087	7,88E-05	11,46	2,39E-08	1,88E-12	1,88E-07	0,13
11	2	0,035	4,92E-04	27,90	4,04E-09	1,99E-12	1,99E-07	0,14
12	9,31E-03	0,0002	2,27E+01	3988,90	1,97E-13	4,49E-12	4,49E-07	0,31

Table 1: The table shows the estimated power carried by the scattered photons at different angles and caught by the solid angle of the photodiode (2 mm of diameter, d is the distance from the PDs to the mirror). For this estimation I have used the assumed BRDF explained in the text and the beam power, fixed at 100 kW. The current generated in the photodiodes is obtained from the responsivity of the detector.

From the obtained values of the power detected by the photodiodes, I can infer the expected current from the manufacturer-provided responsivity curve at the 1064 nm laser frequency (Fig. 26).

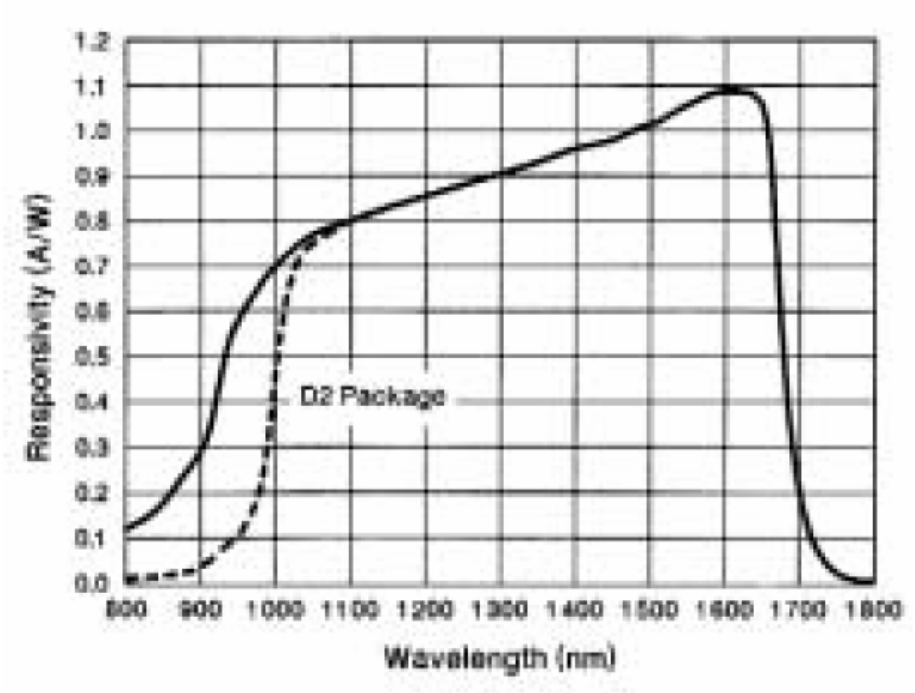

Figure 26: Typical responsivity of the photodetector (C30642 InGaAs) as a function of wavelength. The value which we are interested in is at 1064 nm, which is the wavelength of the laser, and the corresponding responsivity amount to about 0.7 A/W.

From all these measurements, it is quite clear that the noise of the instrumentation employed for detecting the scattering photons is expected to be very low with respect to signal expected from the power carried by the scattered photons and absorbed by the photodetectors.

I want also to emphasize that the measurements performed in Hanford and in Livingston are quite different. In Hanford interferometer, the experiments are performed by using the 3 view ports available to detect the scattered light from outside of the instrument. These ports are located at 45°,

12°, 1° respectively from the ITM, and the photons that exit the interferometer are collected by a photodetector described in Fig. 27.

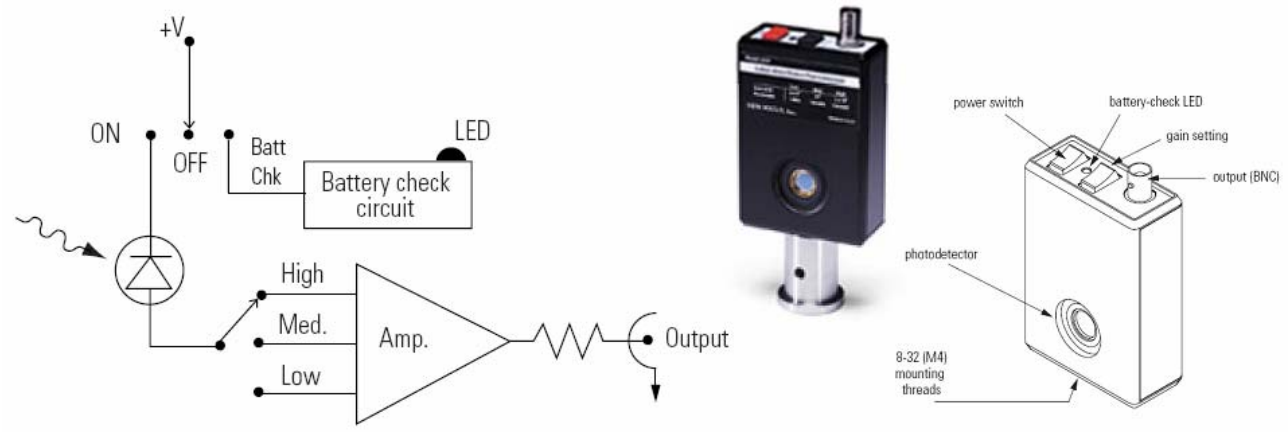

Figure 27: Configuration of the detector employed in the Hanford site for the scattered light measurements. The system includes also three stages of amplification of the signal.

The main difference in the Hanford and Livingston measurements, other than the missing of the measurement at 12°, is due to the different method employed for collecting the photons into the detector. In Hanford it is used a convergent lens system located between the ports and the photodetectors to better select the direction of the photons.

However, this argument is not a crucial difference for, because their purpose is only the estimation of the total losses of the laser total power. The potential problem that some photons may not be come from the mirror (but from a different point in the chamber) is not critical problem because the beam spot is by far the brightest spot in the vacuum chamber. Any spurious reflection would be clearly visible by CCD camera inspection.

Not having to be particularly selective in pointing the diodes, in the proposed in vacuum scatterometer we propose to put on each diode a very simple geometrical collimator (a metal pipe), restricting the diode field of view to the laser spot area. Pointing could be achieved by temporarily removing the PD and looking down the pipe with a miniature camera. The large amount of light and the experience in the external scattering measurement show that in our scatterometer design it is not necessary to put a convergent lens system between the photodiode and the mirror. Also, the expected abundance of light does not require the use of the very low leakage current PD used in these tests (selected for the interferometer signal detection). Much cheaper diodes with moderately higher leakage current can be used.

Conclusions

This work studied an in vacuum scatterometer design able to track the changes of the losses of the laser total power. By having dedicated, in-vacuum, detection diodes we produce a reliable and stable monitor for possible changes in scattering amplitude. In-vacuum diodes are not affected by window cleanliness issues and can hardly be disturbed over the experiment's lifetime. By installing a moderate number of photodiodes in the vacuum chambers it will be possible to give information on possible scatterers that could fall or deposit on the mirror over time. I discussed the characteristics of the photodiodes necessary to detect the scattered photons from the mirror surface, and I calibrated their properties: responsivity, i.e. linear response, saturation level, noise level.

The study shows that, unlike the case of the main signal detection diodes, there is no need to install in-vacuum preamplifier near the diodes and cheap external amplification is sufficient. We also noted that the commercially available diodes are amply sufficient for the task and cheaper diodes with somewhat higher leakage current may be safely used.

Studying the interferometer's arm geometry, I proposed the positioning of the photodiodes in the chamber allowing to measure the shape of the BRDF which is strictly connected to the mirror surface imperfections distributed over the whole frequency spectrum and may help to distinguish between different kinds of scatterers.

References

[1] Yamamoto H., 2007, *LIGO I mirror scattering loss by microroughness*, LIGO-T070082-03-E.